

Journal of Materials Chemistry A

Accepted Manuscript



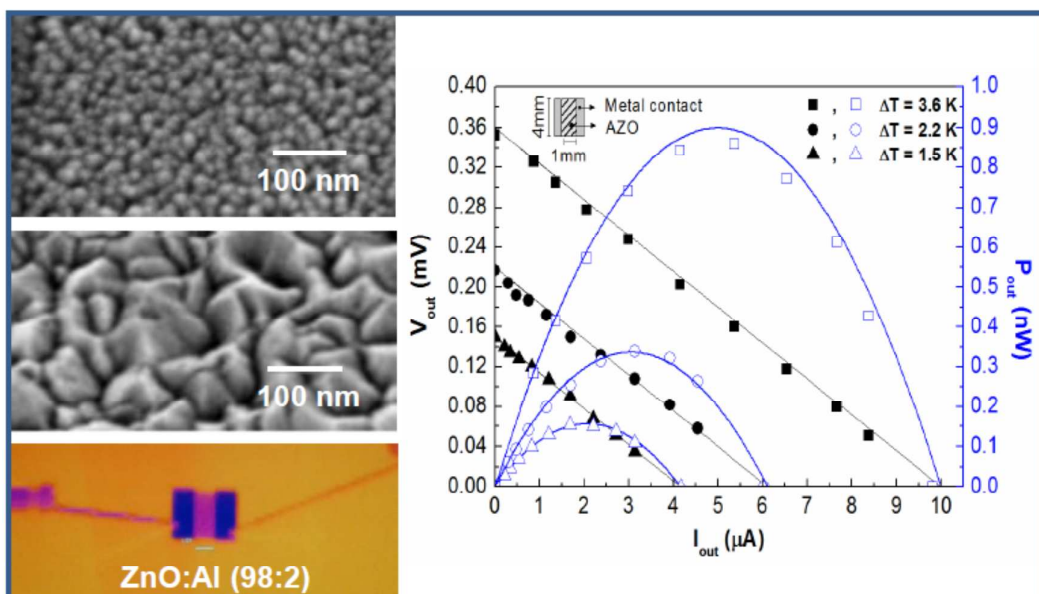
This is an *Accepted Manuscript*, which has been through the Royal Society of Chemistry peer review process and has been accepted for publication.

Accepted Manuscripts are published online shortly after acceptance, before technical editing, formatting and proof reading. Using this free service, authors can make their results available to the community, in citable form, before we publish the edited article. We will replace this *Accepted Manuscript* with the edited and formatted *Advance Article* as soon as it is available.

You can find more information about *Accepted Manuscripts* in the [Information for Authors](#).

Please note that technical editing may introduce minor changes to the text and/or graphics, which may alter content. The journal's standard [Terms & Conditions](#) and the [Ethical guidelines](#) still apply. In no event shall the Royal Society of Chemistry be held responsible for any errors or omissions in this *Accepted Manuscript* or any consequences arising from the use of any information it contains.

This work reports enhanced thermoelectric properties of transparent ZnO:Al thin films. The influence of the ZnO:Al composition, film thickness and deposition method have been studied, and $ZT > 0.1$ has been demonstrated at room temperature.



Transparent Aluminium Zinc Oxide thin films with enhanced thermoelectric properties

Cite this: DOI: 10.1039/x0xx00000x

Received December 2013,

DOI: 10.1039/x0xx00000x

www.rsc.org/

Joana Loureiro*¹, Nuno Neves², Raquel Barros¹, Tiago Mateus¹, Rafael Santos¹, Sergej Filonovich¹, Sebastian Reparaz³, Clivia M. Sotomayor-Torres^{3,4}, Frederic Wyczisk,⁵ Laurent Divay,⁵ Rodrigo Martins¹ and Isabel Ferreira*¹

Improved thermoelectric properties of Aluminum Zinc Oxide (AZO) thin films deposited by radio frequency (RF) and pulsed Direct Current (DC) magnetron sputtering at room temperature are reported. In both techniques films were deposited using sintered and non-sintered targets produced from nanopowders. It is confirmed that both Al doping concentration and films thickness control the thermoelectric, optical and structural properties of these films. Seebeck coefficients up to $-134 \mu\text{V/K}$ and electrical conductivities up to $4 \times 10^4 (\Omega \cdot \text{m})^{-1}$ lead to power factors up to $4 \times 10^{-4} \text{ W/mK}^2$, which is above the state of art for similar materials, almost by a factor of three. The thermoelectric I-V response of an optimized AZO element with a planar geometry was measured and a maximum power output of 2.3 nW, for a temperature gradient of 20 K near room temperature, was obtained. Moreover, the low thermal conductivity ($< 1.19 \text{ W/mK}$) yields a ZT value above 0.1. This is an important result as it is at least three times higher than the ZT found in the literature for AZO, at room temperature, opening new doors for applications of this inexpensive, abundant and environmental friendly material, in a new era of thermoelectric devices.

Introduction

An efficient application of thermoelectric (TE) materials in devices requires materials with high Seebeck coefficient ($S = \Delta V / \Delta T$), low thermal conductivity (k), and low resistivity (ρ) to attain a large figure of merit ($ZT = S^2 T / k\rho$). By nanostructuring materials the ZT value has improved to over 1 at 300 K, taking as example $\text{Bi}_2\text{Te}_3/\text{Sb}_2\text{Te}_3$ superlattices ($ZT > 2$)¹, and n-type PbSeTe ($ZT = 1.5$) materials². Although Te based materials have already captured the market, their application in large volume production processes results unsustainable. Te is the ninth less abundant element^{3, 4} on Earth and since the Te standard modules require roundly 1 kg to produce 1 kW, costs *versus* benefits becomes a problem. Environmental issues concerning the use of Pb and its recyclability leaves no space to explore the commercialization of Pb alloys⁴. Therefore, more abundant and eco-friendly materials/alloys should be studied for thermoelectric applications. Zinc oxide fulfil these requirements and for TE applications it has mainly been explored with bulk dimension and with different dopants: $\text{Zn}_{1-x}\text{M}_x\text{O}$, AZO if $\text{M} = \text{Al}$ and GZO if $\text{M} = \text{Ga}$ ⁵, $\text{Zn}_{1-(x+y)}\text{Ga}_x\text{In}_y\text{O}$ ($x+y=0.007$)⁶ or $\text{ZnAlO}/\text{In-ZnAlO}$

quantum wells multilayers⁷. While bulk TE materials are foremost applied in high power and high temperature regimes, TE thin films (TE-TF) have its main field of application in low temperature and low power consumption electronic devices. Along with a reduction in material usage, TE-TF materials have also other advantages when compared to bulk: higher degrees of freedom as the in-plane geometry can be adapted to the application requirements and thin films can be deposited on flexible substrates as reported in the literature, for example, on polyamide substrates^{8, 9}. Furthermore, AZO thin films have high transmittance in the visible range, so with the improvement of TE properties they would become suitable in transparent electronics devices, among others.

Although the TE properties of AZO thin films are scarce in the literature, some recent results have been reported^{10, 11} showing maximum power factor ($\text{PF} = \sigma S^2$) of $1.5 \times 10^{-4} \text{ W/mK}^2$ with ZT below 0.1 at room temperature. Concerning bulk AZO, the reported power factors are superior (10^{-3} W/mK^2) but as their thermal conductivity is also high¹² the ZT is even lower than 0.1 at room temperature, rising to 0.44 above 1000°C ^{13, 14}.

This work aims the study of the TE properties of TF AZO deposited by RF and pulsed DC magnetron sputtering, using

non-sintered and sintered targets fabricated with AZO nano-powders. The optimized AZO films show a maximum power factor of 3.9×10^{-4} W/mK² and low thermal conductivity (<1.19 W/mK) leading to ZT values above 0.1 at room temperature.

Experimental Section

AZO thin films were deposited by two different methods: RF and pulsed DC magnetron sputtering, both using sintered and non-sintered AZO targets. These targets were fabricated with nano-powders produced by a patented process¹⁵ consisting of high pressure and temperature combined with ultrafast quenching of nanoparticles in a single step, resulting in a more uniform Al distribution in the ZnO matrix compared to the traditional mechanical grinding method. In order to study the influence of Al doping of ZnO on the thermoelectric properties, different ZnO:Al₂O₃ compositions of the sintered targets (99.5:0.5, 99:1, 98.5:1.5, 98:2 wt %) were tested and the TE properties of films with thickness around 250nm were analyzed. A non-sintered AZO target with the optimized Al doping of 2 wt % of Al₂O₃ was also tested in order to study the influence of film thickness between 180 and 900nm. The details about the production process of the nano-powders¹⁵, the targets and the TF depositions using sintered (RF St-AZO) and non-sintered (RF nSt-AZO) targets were given in previous works¹⁶. In those studies the electrical properties were optimized for RF power in the range of 200-250W and working pressure of 1.5-2.0 mTorr. These sample preparation conditions have been kept in the present study.

DC magnetron sputtering is often used in industrial applications to obtain AZO films. Herein we use the same approach focusing on the influence of gas pressure on the TF-TE properties. As in the RF deposition method, both sintered and non-sintered AZO targets were used in the DC method. The electrical properties were optimized for an applied power of 75 W using the non-sintered target and 100 W for the sintered one, in both cases with a pulse break of 8 μ s and a frequency of 10 KHz. When using the sintered target it was necessary to heat the substrate to 473 K and perform a post-deposition thermal treatment at 573 K during 1h in vacuum. The films deposited using a non-sintered target did not require any substrate heating nor post-deposition thermal treatment.

The overall films thickness is in the range of 200 and 350 nm measured with an Ambios XP-200 Profilometer. The structural properties of the films are ascertained by X-ray diffraction (XRD) using a PANalytical X'Pert PRO with CuK α radiation at 45 kV and 40 mA, equipped with a X'Celerator detector. XRD patterns were collected with a scanning step of 0.02° over the angular 2 θ range 10–90°. The surface morphology is observed in a Zeiss Auriga scanning electron microscope equipped with a focused ion beam (SEM-FIB).

To determine the Seebeck coefficient and the power factor, a thermal gradient, ΔT is created by placing the sample between two Peltier modules, TEC1-12707, each connected to an independent power source. ΔT is monitored through a thermal

image taken with a FLIRA310 thermal camera. The corresponding thermovoltage, ΔV , is measured using a nano voltmeter Agilent 34420A while keeping the average temperature constant at 293 K. The carriers Hall mobility (μ), electrical conductivity (σ) and concentration (N) were measured through a Hall-effect measurement system (Bio Rad HL 5500) using the van der Pauw configuration.

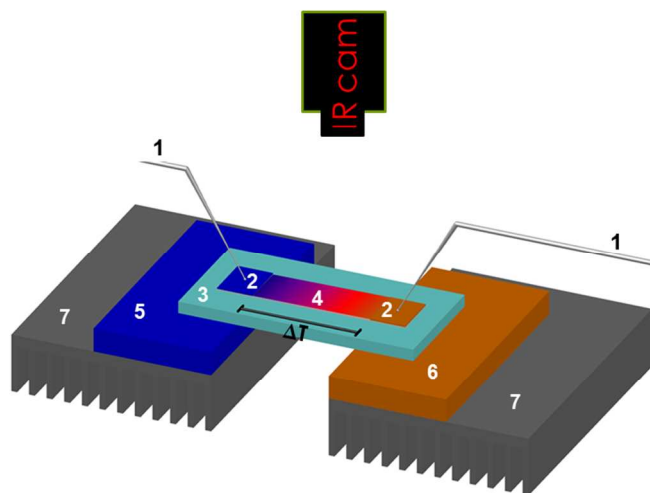


Figure 1. Home-made setup scheme for the Seebeck measurement of the thin films. 1) Nano-Voltmeter probes, 2) Al contacts, 3) Glass substrate, 4) AZO thin film, 5) Peltier (cold side), 6) Peltier (hot side), 7) dissipators.

Auger depth profiles were measured with 3 kV electron beam acceleration, using a PHI 680 Auger Nanoprobe from Physical Electronics, and the argon ion energy was 2 keV for sputtering. The average sputtering rate was between 8 and 10 nm/min, depending on the material.

Thermal conductivity measurements were performed using the 3ω method with a home-built setup suitable for measurements between 25 and 300 K. Special samples were grown on Si substrates in order to determine accurately the cross-plane thermal conductivity of the AZO thin films. The AZO films were electrically isolated from the 3ω resistor by depositing a 20 nm Al₂O₃ film by atomic layer deposition (ALD). The deposition of the insulating layer was performed at 100 °C in ozone atmosphere. An Au resistor 1 mm long, 10 μ m wide and 100 nm thick was deposited on the samples and served as heater and thermometer. We note that this technique is suitable to determine the thermal conductivity of thin films provided that the thermal conductivity of the substrate is larger by a factor of 10 compared to that of the thin films as discussed in detail by Cahill¹⁷. The experimental accuracy for the present measurements is between 5 to 10%.

Results and Discussion

The influence of Al doping on S, PF and σ of films obtained from rf St-AZO targets with different compositions are shown in Fig. 2. As observed in Fig. 2b, the |S| value decreases from

114 μ V/K to 90 μ V/K while the electrical conductivity increases from 6×10^3 to 4×10^4 ($\Omega \cdot \text{m}$)⁻¹ leading to an increase of the PF from 8.1×10^{-5} W/mK² to 3.9×10^{-4} W/mK² as the Al content rises (Fig. 2a). In a previous detailed study focused on the electrical properties of these films it has been shown that the mobility of the majority carriers (μ), decreases from 16.2 to 12.8 cm²/Vs and the concentration (n) increases from 1.36×10^{20} to 4.78×10^{20} cm⁻³, when the Al₂O₃ content in the target increases from 0.5 to 2.0 wt %¹⁸. Therefore, we may correlate the improvement of electrical conductivity with the increase of carrier concentration, while the drop of S can be attributed to the higher metal content. In Fig. 2c and d the differences between the surface morphology of films produced with 0.5 and 2 wt % of Al₂O₃ content in the target are clearly visible: higher Al content results in films with smaller grain sizes, which can be considered as scattering centers for electrons and phonons, helping to lower the thermal conductivity.

films have a typical pattern of hexagonal wurtzite structure (ZnO) with a (002) main diffraction peak at $2\theta=34^\circ$. The crystallite size in the films decreases from 52 to 29 nm as the target Al₂O₃ content increases from 0.5 to 2 wt % (Fig. 2c and d). From Seebeck coefficient measurements the type of the majority carriers was established. Since S is negative in all deposited films they exhibit typical n-type semiconductor behavior, in agreement with Hall-effect data. Concerning optical transparency, all the films have a transmittance above 80 % in the visible spectral range^{16, 18}.

The influence of films thickness (d) on the thermoelectric properties (S and PF) of films deposited by the RF process using a non-sintered ZnO:Al₂O₃ (98:2 wt %) target, which is the composition that gave the best results for sintered AZO films, is shown in Fig. 3.

The increase of d lead to a decrease in S, and since the electrical conductivity is uphold between 2 and 4×10^4 ($\Omega \cdot \text{m}$)⁻¹

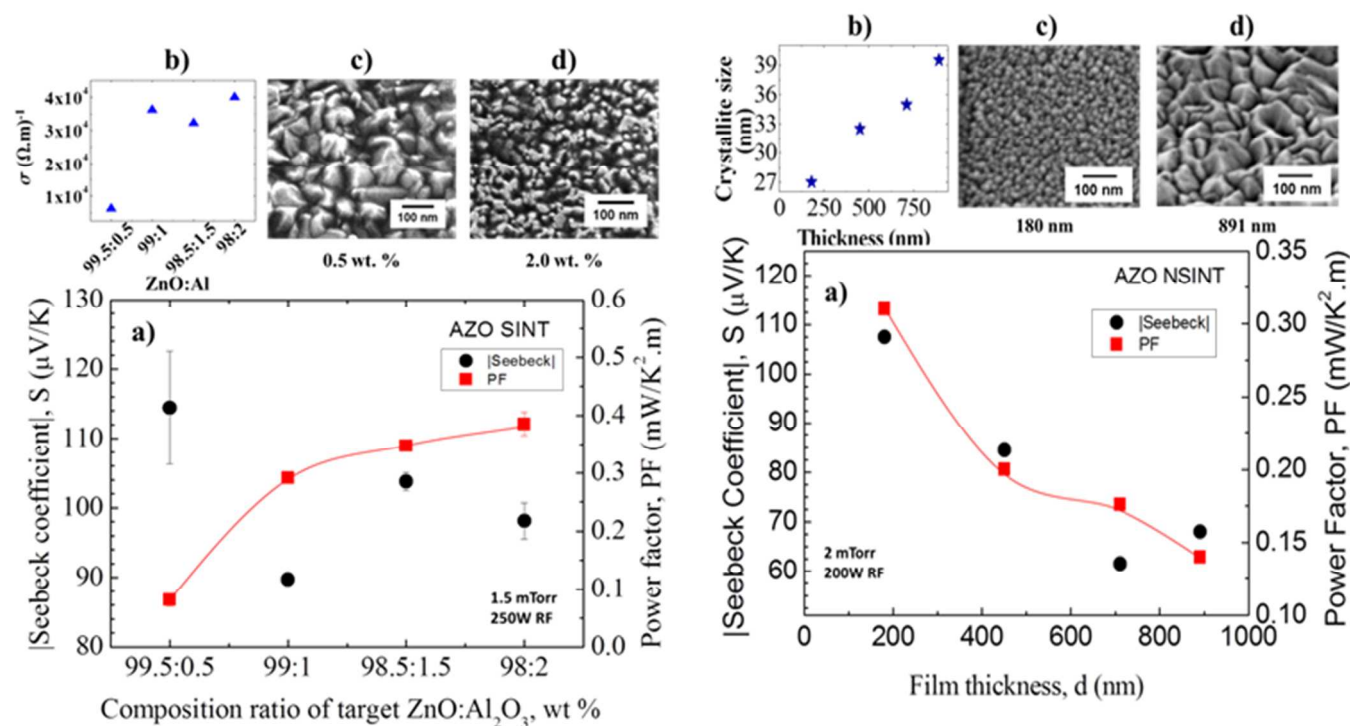


Figure 2. Absolute value of S (circles), PF (squares) (a) and electrical conductivity (triangles) (b) as a function of the composition ratio of the films produced with a sintered AZO target (St-AZO) at a rf-magnetron power of 250 W and a working pressure of 1.5 mTorr. SEM micrographs of the samples with the lowest ratio and highest ratio are also shown in (c) and (d).

However, if the interfaces of these smaller grains are incoherent it may reduce the electron mobility since the scattering of electrons increases and consequently the electrical conductivity drops¹⁹.

As in this case the electrical conductivity is enhanced when Al doping in AZO targets increases (Fig. 2b) thus it is possible to infer that this doping increase has been verified also in the deposited films, leading to an increase of the carriers concentrations, and consequently on the electrical conductivity. Independently of the Al content of targets, all the produced

Figure 2. Absolute value of S (circles), PF (squares) (a) and crystallite sizes (b) as a function of the films produced with a non-sintered AZO target (nSt-AZO) at a rf-magnetron power of 200 W and a working pressure of 2 mTorr. SEM micrographs for the smallest and largest thickness are also shown in (c) and (d).

the PF follows the trend of S decreasing from 3×10^{-4} W/mK² ($d=180$ nm) to 1.4×10^{-4} W/mK² ($d=890$ nm) (as plotted in Fig. 3a). This behaviour can be correlated to the increase of the crystallite sizes from 27 to 40 nm, confirmed by XRD data and SEM images (Fig. 3c and 3d).

As observed in a previous work²⁰ and by other authors, the decrease in grain sizes also benefits the thermoelectric properties due to potential barrier scattering at grains boundaries^{21, 22} which may explain why the thinnest film ($d=180$ nm) with smaller grain sizes have the highest Seebeck coefficient values.

However, the scattering of electrons does not increase with these interfaces as the electron mobility (and consequently the electrical conductivity) is almost unchanged (staying around 7 cm²/Vs) for the range of thicknesses studied. A similar trend has been observed by other authors in Al doping TiO₂.²³

In the above discussion possible dispersion effect along the film thickness of Al dopant have not been considered since the Auger depth profile reveals that Al is uniformly distributed along the cross section of the nSt-AZO and St-AZO films, as shown in Fig. 4. In both profiles the Al concentration is practically the same and evaluated to be around 3 at. %, without calibration, which agrees well with the 2 wt. % of the target. The non-stoichiometry of ZnO and SiO₂ is due to phenomena such as reduction under electron beam deposition and/or preferential sputtering for the binary compound. A small carbon peak is visible near the surface that is attributed to surface contamination.

According to Wiedeman-Franz law: $k_{\text{EL-WF}} = L_0 \sigma T$, where L_0 is the Lorenz number, $\pm 2.44 \times 10^{-8} \text{ V}^2 \text{K}^{-2}$ for metals, the AZO thin film showing the highest electrical conductivity

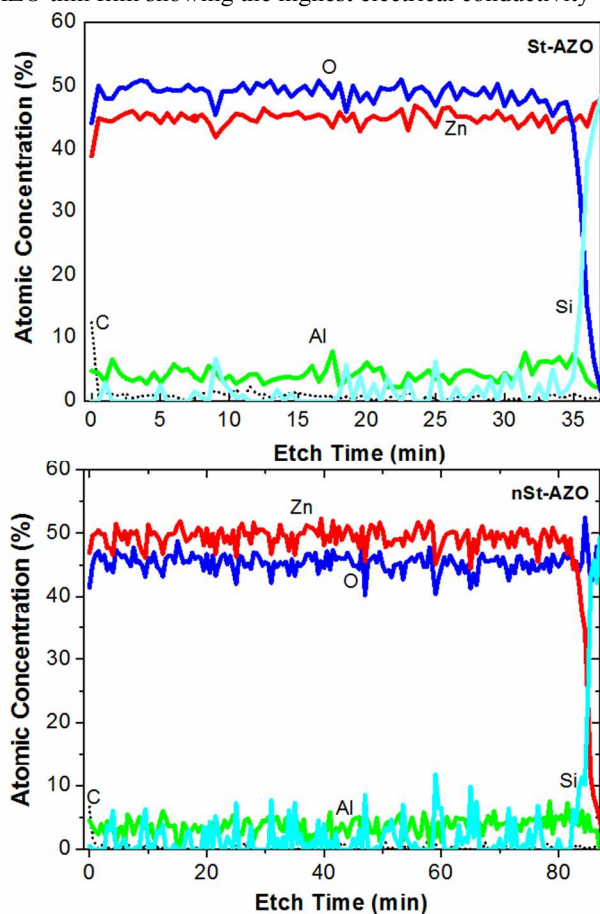


Figure 4. AES atomic concentration spectra of two AZO thin films. Left: Film deposited by RF with the St-AZO target (400nm thick); Right: Film deposited by RF with the nSt-AZO target (700nm thick). The sputtering rate was between 8 and 10 nm/min.

($4 \times 10^4 \text{ } (\Omega \text{m})^{-1}$) will have the highest thermal conductivity, k_{EL} , of 0.34 W/mK.^{1, 24} The thermal conductivity represents the heat transfer in the material by both electrons and phonons: $k = k_{\text{EL}} + k_{\text{PH}}$. Other important factors such as material structure, grain sizes, defects, mean free path of carriers, phonons scattering, among others, strongly influence the thermo and electrical performances. As discussed before, the grain sizes of AZO diminish together with the films thickness, leading to an expected drop in thermal conductivity, as mentioned by other authors^{12, 25, 26}. This drop can be associated to grain interfaces since they are good scattering centers for phonons, thus decreasing the thermal conductivity. In fact, it has been shown that the thermal conductivity of the ZnO thin films is dominated by the intrinsic thermal conductivity, which is a function of grain size²³.

The decrease of k with thickness also arises from the scattering by lattice impurities²³, which lead to a charge state different from the perfect crystal, and frozen-in structural defects of films, that will most likely scatter electrons and reduce their mobility. The temperature dependence of the combined electrons and phonons on thermal conductivity was measured in a 700 nm thick AZO film with $4 \times 10^4 \text{ } (\Omega \text{m})^{-1}$ electrical conductivity and is shown in Fig. 5. At 300 K, $k = 1.19 \text{ W/mK}$ which is higher than the previous calculated k_{EL} ,

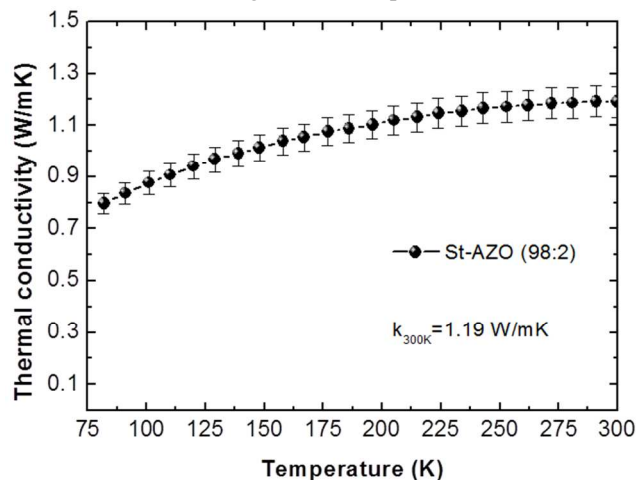


Figure 5. Thermal conductivity as a function of temperature for an AZO (98:2) thin film, with $d=700 \text{ nm}$, deposited by RF using a St-AZO target.

showing a reduced phonon contribution. The k value found in the literature for bulk AZO is between 30 and 40 W/mK^{13, 14, 27}. Recent reports have confirmed a decrease on the thermal conductivity of ZnO films along with the reduction of the film thickness and grains sizes²⁵. In that work, a thermal conductivity of 2.3 W/mK is reported for films with grain sizes higher than 35 nm. As our AZO films have even smaller grains, a lower k value was expected and experimentally confirmed.

Based on the previously discussed behaviour of thermal conductivity with thickness, the value of k for the deposited films with $d < 700 \text{ nm}$ should be even smaller than 1.19 W/mK. However, due to the difficulties in measuring k for very thin

films we have considered this value for all samples, keeping in mind that this may give an under estimate ZT value.

Since pulsed DC magnetron sputtering technique is the most used technique in industry, preliminary tests have been performed to deposit AZO thin films through this technique, using sintered targets or non-sintered targets. In the first deposition trials, the influence of power, pressure, type of target and distance to target upon the TE properties of the AZO thin films have been evaluated and the best results are shown in table 1.

The AZO films deposited by pulsed DC using a sintered target show a typical hexagonal wurtzite structure of ZnO with

a (002) main diffraction peak at $2\theta=34^\circ$ as observed in the samples produced by the RF method. However, other diffraction peaks at $2\theta=35.2^\circ$ (011), $2\theta=46.7^\circ$ (012) and $2\theta=61.8^\circ$ (013) appear after the post-deposition annealing step and/or substrate heating during the deposition.

The films produced from a non-sintered target, also show the typical ZnO wurtzite structure but with two peaks (002), at $2\theta=34.1^\circ$ and (004) $2\theta=72^\circ$. The crystallite sizes related to main peak (002) are shown in table 1 and were calculated from Scherrer's formula. Comparing the DC and RF method, and for the deposition conditions used, we obtain better PF for AZO films produced by RF method.

Table 1 - Properties of optimized AZO films produced by RF and pulsed DC sputtering methods with sintered (St) and not sintered (nSt) AZO targets with ZnO:Al₂O₃ content of 98:2 wt %.

Deposition Method - Target	P _{dep} (mtorr)	Power (W)	D (nm)	Crystallite size (nm)	μ _e (cm ² /Vs)	N (cm ⁻³)	σ (Ωm) ⁻¹	S (μV/K)	PF (W/mK ²)
RF - St	1.5	250	240	29	13	1.9×10 ²⁰	4.0×10 ⁴	-98	3.9×10 ⁻⁴
RF - nSt	2.0	200	181	27	7.1	3.4×10 ²⁰	3.9×10 ⁴	-90	3.1×10 ⁻⁴
DC - St	2.2	100	357	9.1	3.4	1.1×10 ²⁰	6.1×10 ³	-134	1.1×10 ⁻⁴
DC - nSt	3.2	75	200	9.6	8.4	1.8×10 ¹⁹	2.4×10 ³	-132	4.2×10 ⁻⁵

Table 2 - Comparison of the TE data of AZO films produced in this work with those of films and bulk material published in the literature. For the ZT* values denoted with * there was no information on the thermal conductivity, therefore, ZT was calculated using the same k as measured in the thin films presented in this work, namely 1.19 W/mK, for comparison purposes. For the ZT** values denoted with ** there was no information concerning the k values and ZT was calculated using k from literature for bulk AZO, namely 30 W/mK.

ZnO:Al ₂ O ₃ wt %	Dep. Method	d (nm)	T _{work} (K)	σ (Ωm) ⁻¹	K (W/mK)	S (μV/K)	PF (W/mK)	ZT	Ref
98:2	RF (St-AZO target)	240	RT	4×10 ⁴	<1.19	98	3.9×10 ⁻⁴	>0.1	our results
98.5:1.5	DC	120	RT	10 ⁴	-	62	1.3×10 ⁻⁴	~0.03*	11
98.5:1.5	DC	103	RT	10 ⁴ - 10 ⁵	-	68	1.5×10 ⁻⁴	~0.04*	28
97.3:2.7	DC	716	RT	10 ⁴	-	99	1.5×10 ⁻⁴	~0.04*	10
98:2	PLD	500	RT	10 ⁴	-	65	1.3×10 ⁻⁴	~0.03*	29
98:2	Solid-state reaction (pressure)	bulk	RT	10 ⁴ - 10 ⁵	40.2	100-150	8×10 ⁻³	6×10 ⁻³	27
98:2	Solid-state reaction (pressure)	bulk	RT	10 ⁵	-	62.5	3.8×10 ⁻⁴	10 ^{-3**}	30
99:1	RF plasma and hot pressed	bulk	RT	10 ⁴	28	37	1.3×10 ⁻⁴	2×10 ⁻³	31
97:3	Chemical co-deposition and pressed	bulk	373	10 ⁴	14	200	5×10 ⁻⁴	~0.02	32
96:4	Spark plasma sintering	bulk	675	10 ⁴	2	88	3.2×10 ⁻⁴	0.085	14
98:2	Spark plasma sintering	bulk	1173	10 ⁴	5.15	120	8×10 ⁻⁴	0.17	33

However the films produced by pulsed DC method, have smaller grain sizes, independently of the target used, which suggest better TE properties. Indeed, in these samples, S is slightly enhanced, but the electrical conductivity is one order of magnitude inferior and so PF is also lower. It is important to emphasize that these are preliminary results and that further efforts should be made to improve the TE results and to understand better the physic mechanisms involved. The TE results achieved here in films deposited with non-sintered targets using pulsed DC technique are already close to those reported in the literature (as shown in table 2), demonstrating that it is possible to obtain high quality films from non-sintered

targets produced with AZO nano-powders both by DC or RF sputtering techniques.

Therefore, the obtained results prove that non-sintered targets based on nano-powders can be used both in RF and pulsed DC magnetron sputtering systems to fabricate AZO thin films with advanced thermoelectric properties. Most importantly, by eliminating the sintering step, fabrication time and energy costs will be both reduced making the production process of targets more economic.

To evaluate the power generation performance of an AZO TF element, we measured the output voltage and power of the optimized films by changing the load resistance and

temperature gradient. The obtained curves are shown in Fig. 6. The current–voltage characteristic of the thermoelectric element is linear, as described by the equation $V_{\text{out}} = S\Delta T - IR_{\text{int}}$ where V_{out} is the output voltage at the load resistance terminals, I is the total current flowing through the circuit and R_{int} is the internal resistance of the TE element. The output power is described by the equation $P_{\text{out}} = S\Delta TI - I^2R_{\text{int}}$. In Fig. 6 both the output voltage and output power of the TE elements are shown for three thermal gradients (1.5, 2.2 and 3.6 K) at room temperature. The simulated curves fit well the experimental data.

The thermoelectric element has its maximum power output when the load resistance is equal to the internal resistance R_{int} and the current at the point of maximum power is half of the short circuit current. In this case, the maximum power of the thermoelectric element with at a certain temperature gradient, is $P_{\text{max}} = S^2\Delta T^2/4R_{\text{int}}$ ³⁴.

For the three ΔT measurements, the obtained P_{max} and the current and voltage that maximizes the output power, $I_{P_{\text{max}}}$ and $V_{P_{\text{max}}}$, are shown in Table 3. Based on the theoretical models, a maximum power output of 43.4 nW is expected for a $\Delta T=25\text{K}$. It is important to emphasize that these results have been obtained for a single n-type TE element. Although this power output power is small for most applications, it is already comparable to full devices comprising 100 thin film thermocouples of $\text{Sb}_2\text{Te}_3/\text{Bi}_2\text{Te}_3$, also with planar geometry, which for $\Delta T = 20\text{K}$ have a maximum power output of 7 nW³⁵. By connecting this n-type thermoelectric element with a compatible p-type element, such as $\text{Cr:V}_2\text{O}_5$ ²⁰ and using an appropriate combination of series and parallel interconnections between the TE elements it will be possible to design devices with higher output powers to meet the needs of low power TE modules applications.

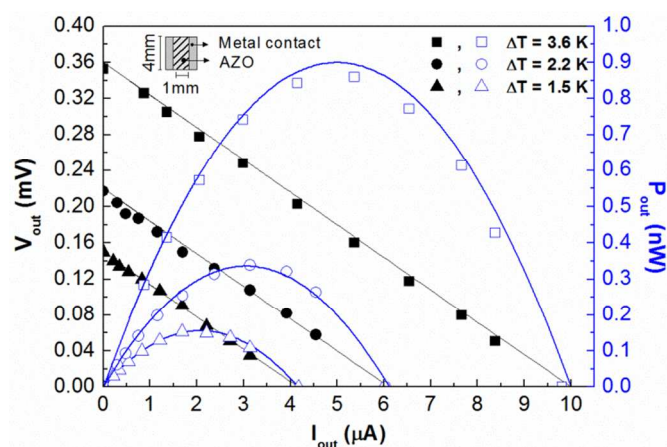


Figure 6. Output voltage (solid symbols) and output power (opened symbols) for three temperature gradients: 1.5 K (triangles), 2.2 K (circles) and 3.6 K (squares) versus output current, for a single n-type AZO (98:2 wt %) thin film TE element, with an area of 4 mm x 1 mm, deposited by rf using a sintered target. The solid lines are theoretical calculations.

Moreover, it has been demonstrated that similar results are obtained in films made with sintered and non-sintered targets

both using RF and pulsed DC sputtering. The relevance of this conclusion is the elimination of the sintering step, and therefore the reduction in fabrication costs, with direct consequence in lowering thermoelectric thin film modules cost, making them more appealing for large area TE applications.

Table 3: Maximum output power generation (P_{max} , $I_{P_{\text{max}}}$ and $V_{P_{\text{max}}}$) of a single n-type AZO (98:2 wt %) thin film element (area: 4 mm x 1 mm) deposited by rf using a sintered target, for the three measured temperature gradients, 1.5 K, 2.2 K and 3.6 K, and for a simulated (*) gradient, 25 K

ΔT (K)	P_{max} (nW)	$I_{P_{\text{max}}}$ (μA)	$V_{P_{\text{max}}}$ (mV)
1.5	0.16	2.08	0.08
2.2	0.34	3.06	0.11
3.6	0.90	5.00	0.18
25*	43.40*	34.7*	1.25*

Conclusions

We have demonstrated that AZO films produced by RF magnetron sputtering of targets made with nano-powders have room temperature thermoelectric properties above the state-of-the-art, with a $\text{PF} = 4 \times 10^{-4} \text{ W/mK}^2$ and $\text{ZT} > 0.1$. These results were achieved in films with crystallite sizes less than 30nm. The importance of crystallite/grain sizes for TE properties has been shown. They are highly transparent and dependent on the deposition conditions and especially on the Al doping concentration.

Acknowledgements

This work was partially supported by the Portuguese Agency of Innovation (Adi) under project QREN/3435-Nanoxides, by the Portuguese Science and Technology Foundation (FCT), the Ministry for Education and Science (MEC), under PEST-C/CTM/LA0025/2011 (Strategic Project - LA 25 - 2011-2012), the Spanish Plan Nacional I+D project TAPHOR (MAT-2012-31392), the Spanish CONSOLIDER project nanoTHERM (CDS2010-00044) and mainly by the NANOTEG project: ENIAC/002/2010.

Notes

- ¹ CENIMAT/I3N, Departamento de Ciência dos Materiais, Faculdade de Ciências e Tecnologia, FCT, Universidade Nova de Lisboa and CEMOP-UNINOVA, 2829-516 Caparica, Portugal.
- ² INNOVNANO, Materiais Avançados SA, 3040-570 Antanhol, Portugal
- ³ Catalan Institute of Nanoscience and Nanotechnology ICN2, Campus UAB, Edifici ICN2, 08193 Bellaterra (Barcelona), Spain.
- ⁴ Catalan Institution for Research and Advanced Studies ICREA, 08010 Barcelona, Spain.
- ⁵ Thales Research and Technology, Palaiseau Cedex 91767, France.

References

1. R. Venkatasubramanian, E. Siivola, T. Colpitts and B. O'Quinn, *Nature*, 2001, **413**, 597-602.

2. C. J. Vineis, A. Shakouri, A. Majumdar and M. G. Kanatzidis, *Advanced Materials*, 2010, **22**, 3970-3980.
3. P. Vaqueiro and A. V. Powell, *Journal of Materials Chemistry*, 2010, **20**, 9577.
4. B. K. Meyer and P. J. Klar, *physica status solidi (RRL) - Rapid Research Letters*, 2011, **5**, 318-323.
5. K.-H. Jung, S.-M. Choi, C.-H. Lim, W.-S. Seo and H.-H. Park, *Surface and Interface Analysis*, 2012, **44**, 1507-1510.
6. H. Takemoto, H. Kawakami, M. Saito and H. Yamamura, *Procedia Engineering*, 2012, **36**, 434-438.
7. S. Teehan, H. Efstathiadis and P. Haldar, *Journal of Alloys and Compounds*, 2012, **539**, 129-136.
8. M. Takeda, M. Terui, N. Takahashi and N. Ueda, *Journal of Solid State Chemistry*, 2006, **179**, 2823-2826.
9. R. Izaki, N. Kaiwa, M. Hoshino, T. Yaginuma, S. Yamaguchi and A. Yamamoto, *Applied Physics Letters*, 2005, **87**, 243508.
10. P. Fan, Y.-z. Li, Z.-h. Zheng, Q.-y. Lin, J.-t. Luo, G.-x. Liang, M.-q. Zhang and M.-c. Chen, *Applied Surface Science*, 2013.
11. L. Li, L. Fang, X. M. Chen, J. Liu, F. F. Yang, Q. J. Li, G. B. Liu and S. J. Feng, *Physica E: Low-dimensional Systems and Nanostructures*, 2008, **41**, 169-174.
12. T. M. Tritt, *Thermal Conductivity: Theory, Properties and Applications*, Springer, 2004.
13. P. Jood, R. J. Mehta, Y. Zhang, G. Peleckis, X. Wang, R. W. Siegel, T. Borca-Tasciuc, S. X. Dou and G. Ramanath, *Nano Letters*, 2011, **11**, 4337-4342.
14. N. Ma, J. F. Li, B. P. Zhang, Y. H. Lin, L. R. Ren and G. F. Chen, *Journal of Physics and Chemistry of Solids*, 2010, **71**, 1344-1349.
15. J. M. Calado, 2009.
16. N. Neves, R. Barros, E. Antunes, J. Calado, E. Fortunato, R. Martins and I. Ferreira, *Journal of the European Ceramic Society*, 2012, **32**, 4381-4391.
17. D. G. Cahill, *Review of Scientific Instruments*, 1990, **61**, 802-808.
18. N. Neves, *Solar energy materials and solar cells*, 2013 waiting for approval.
19. T. Kamiya, K. Nomura and H. Hosono, *Science and Technology of Advanced Materials*, 2010, **11**, 044305.
20. J. Loureiro, R. Santos, A. Nogueira, F. Wyczisk, L. Divay, S. Reparaz, F. Alzina, C. M. Sotomayor Torres, J. Cuffe, F. Montemor, R. Martins and I. Ferreira, *Journal of Materials Chemistry A*, DOI:10.1039/C3TA15168A, 2014.
21. K. Kishimoto and T. Koyanagi, *Journal of Applied Physics*, 2002, **92**, 2544.
22. C.-H. Kuo, H.-S. Chien, C.-S. Hwang, Y.-W. Chou, M.-S. Jeng and M. Yoshimura, *Materials Transactions*, 2011, **52**, 795-801.
23. L. Xu, M. P. Garrett and B. Hu, *The Journal of Physical Chemistry C*, 2012, **116**, 13020-13025.
24. A. J. Minnich, M. S. Dresselhaus, Z. F. Ren and G. Chen, *Energy & Environmental Science*, 2009, **2**, 466.
25. Y. Xu, M. Goto, R. Kato, Y. Tanaka and Y. Kagawa, *Journal of Applied Physics*, 2012, **111**, 084320.
26. P. Nath and K. L. Chopra, *Thin Solid Films*, 1973, **18**, 29-37.
27. M. Ohtaki, T. Tsubota, K. Eguchi and H. Arai, *Journal of Applied Physics*, 1996, **79**, 1816.
28. L. Li, L. Fang, X. J. Zhou, Z. Y. Liu, L. Zhao and S. Jiang, *Journal of Electron Spectroscopy and Related Phenomena*, 2009, **173**, 7-11.
29. P. Mele, S. Saini, H. Honda, K. Matsumoto, K. Miyazaki, H. Hagino and A. Ichinose, *Applied Physics Letters*, 2013, **102**, 253903.
30. D. Bérardan, C. Byl and N. Dragoë, *Journal of the American Ceramic Society*, 2010, **93**, 2352-2358.
31. H. Cheng, X. J. Xu, H. H. Hng and J. Ma, *Ceramics International*, 2009, **35**, 3067-3072.
32. X. Qu, W. Wang, S. Lv and D. Jia, *Solid State Communications*, 2011, **151**, 332-336.
33. L. Han, N. V. Nong, L. T. Hung, T. Holgate, N. Pryds, M. Ohtaki and S. Linderoth, *Journal of Alloys and Compounds*, 2013, **555**, 291-296.
34. I. Sateikis, R. Ambrulevicius and S. Lynikiene, *Electronics & Electrical Engineering*, 2010, **10**, 113-116.
35. L. Francioso, C. De Pascali, I. Farella, C. Martucci, Creti, x, P., P. Siciliano and A. Perrone, *Sensors*, 2010 IEEE, 2010.